



Division - Soil Processes and Properties | Commission - Soil Chemistry

# Model of inner-sphere adsorption of oxyanions in goethite - Why is phosphate adsorption more significant than that of sulfate?

Carla Gomes de Albuquerque<sup>(1)\*</sup> , Fabiana Gavelaki<sup>(1)</sup> , Vander Freitas Melo<sup>(1)</sup>   
Antônio Carlos Vargas Motta<sup>(1)</sup> , Aldo José Gorgatti Zarbin<sup>(2)</sup>  and Caroline Mariano Ferreira<sup>(2)</sup> 

<sup>(1)</sup> Universidade Federal do Paraná, Departamento de Solos e Engenharia Agrícola, Pós-Graduação em Ciência do Solo, Curitiba, Paraná, Brasil.

<sup>(2)</sup> Universidade Federal do Paraná, Departamento de Química, Pós-Graduação em Química, Curitiba, Paraná, Brasil.

**ABSTRACT:** Phosphorus availability in soils is low due to its strong retention by inner-sphere complexation on minerals in the clay fraction with pH-dependent charges, such as goethite. On the other hand, sulfur has greater availability because it is retained mainly by electrostatic attraction. We evaluated the intensities of the inner-sphere complexation of orthophosphate and sulfate ( $\text{H}_2\text{PO}_4^-/\text{HPO}_4^{2-}$  and  $\text{SO}_4^{2-}$  - generically treated as  $\text{PO}_4$  and  $\text{SO}_4$ ) under different experimental conditions (pH, goethite purity, and contact times) on synthetic goethite samples to establish the mechanisms and models involved in those bonds. Inner-sphere  $\text{PO}_4$  and  $\text{SO}_4$  were extracted using both  $\text{HNO}_3$  1 mol L<sup>-1</sup> and USEPA 3051A methods. Inner-sphere complexation of  $\text{PO}_4$  and  $\text{SO}_4$  was highest at pH 5 in relation to pH 9. Attenuated total reflectance/Fourier transform infrared spectroscopy (ATR-FTIR) spectra showed inner-sphere complexation bands of  $\text{PO}_4$  on goethite in the protonated binuclear bidentate (pH 5) and deprotonated binuclear bidentate (pH 9) forms. Inner-sphere complexation of  $\text{PO}_4$  was much more expressive than that of  $\text{SO}_4$ . Phosphorus and sulfur oxyanions displace the diprotonated ferrol ligand ( $-\text{OH}_2^{+0.5}$  in  $-\text{FeOH}_2^{+0.5}$ ), while the  $-\text{OH}^{-0.5}$  in the  $-\text{Fe}-\text{OH}^{-0.5}$  group are only displaced by  $\text{PO}_4$ . The  $-\text{O}^{-1.5}$  ligand in  $\text{Fe}-\text{O}^{-1.5}$  group is not displaced by  $\text{PO}_4$  or  $\text{SO}_4$ . The high surface negative charge density of  $\text{PO}_4$  defined its higher activation energy for exchanging  $-\text{OH}_2^{+0.5}$  and  $-\text{OH}^{-0.5}$  on the goethite surface in relation to  $\text{SO}_4$ . The proposed model can be used to reduce inner sphere phosphate adsorption in soils and improve P fertilization efficiency for farming.

**Keywords:** iron oxyhydroxides, ligand exchange, activation energy, ferrol groups, zero-point charge.

**\* Corresponding author:**

E-mail: carlaalbuquerque@ufpr.br

**Received:** December 04, 2021

**Approved:** February 09, 2022

**How to cite:** Albuquerque CG, Gavelaki F, Melo VF, Motta ACV, Zarbin AJG, Ferreira CM. Model of inner-sphere adsorption of oxyanions in goethite - Why is phosphate adsorption more significant than that of sulfate? Rev Bras Cienc Solo. 2022;46:e0210146.

<https://doi.org/10.36783/18069657rbcs20210146>

**Editors:** José Miguel Reichert  and Leônidas Azevedo Carrijo Melo .

**Copyright:** This is an open-access article distributed under the terms of the Creative Commons Attribution License, which permits unrestricted use, distribution, and reproduction in any medium, provided that the original author and source are credited.



## INTRODUCTION

Iron and aluminum oxides, 1:1 phyllosilicates (kaolinite), and organic matter are colloidal particles that have variable electrical charges due to the exposure of their ionizable hydroxyl groups (protonation and deprotonation) (Anderson and Sposito, 1991; Fang et al., 2019; Zhao et al., 2019). Iron oxides (oxides, hydroxides, and oxy-hydroxides) are very common in highly weathered soils (Cornell and Schwertmann, 2003).

Generally, goethite ( $\alpha$ -FeOOH) is the most abundant Fe oxide in the soil and has high reactivity (Schwertmann and Taylor, 1989). Due to the lower electronegativity of Fe in relation to Si (present in kaolinite) or Al (kaolinite and gibbsite), there is a greater approximation of the electronic pair of the Fe-O bond towards oxygen in superficial ferrol groups (Fe-OH), which makes hydrogen weakly ionizable (with lower acidity). The ferrol group has a high pH of point of zero charge ( $\text{pH}_{\text{ZPC}}$ ) (between 8 and 9) (Alleoni et al., 2009; Costa and Bigham, 2009; Kosmulski, 2018). As the pH of soils is normally below this  $\text{pH}_{\text{ZPC}}$  range, goethite has a predominance of positive charges (anion exchange capacity - AEC), which facilitates outer-sphere complexation of phosphates and sulphates and other negatives ions as well as molecules having agronomic, pharmaceutical, and environmental importance (Gérard, 2016; Zhao et al., 2017; Essington and Stewart, 2018; Stolze et al., 2019).

Inorganic P in the soil is normally strongly inner sphere adsorbed to Fe and Al oxides as an oxyanion ( $\text{H}_2\text{PO}_4^-/\text{HPO}_4^{2-}$  - generically treated as  $\text{PO}_4$ ) and is not readily available to plants, reducing the efficiency of phosphate fertilizers (Roberts and Johnston, 2015; Gérard, 2016). Inner sphere adsorption on Fe and Al oxides is one of the main mechanisms reducing  $\text{PO}_4$  leaching and its loss to ground and surface waters in humid tropical areas (Li and Arai, 2020). After being electrostatically attracted (outer sphere complexation), the  $\text{PO}_4$  in the Stern layer loses its hydration water and covalently bonds to the surfaces of Fe and Al oxides in monodentate or bidentate configurations (Tejedor-Tejedor and Anderson, 1990; Persson et al., 1996; Arai and Sparks, 2001; Luengo et al., 2006; Kubicki et al., 2012). The same mechanism can occur with ( $\text{SO}_4^{2-}$  - generically treated as  $\text{SO}_4$ ) (the main source of S for plants) (Lefèvre, 2004; Scherer, 2009; Hinkle et al., 2015; Gu et al., 2016). Even with evidence of monodentate inner sphere complexation (Hug, 1997), it is assumed that outer sphere complexation predominates between  $\text{SO}_4$  and Fe and Al oxides, while  $\text{PO}_4$  is retained by inner-sphere complexation. The ability of  $\text{PO}_4$  to engage in inner sphere binding is due to its ease of displacing hydroxylated goethite ligands - which does not happen as easily with  $\text{SO}_4$ . Several studies of oxyanion adsorption on synthetic goethite have been published (Kim et al., 2011; Kubicki et al., 2012; Waiman et al., 2013; Abdala et al., 2015; Hinkle et al., 2015), but there is still no information available concerning mechanisms that could explain the differences in the intensities of the bonds between  $\text{PO}_4$  and  $\text{SO}_4$  and soil minerals with pH dependent charges.

Most studies propose modeling models such as the diffuse layer model (DLM) and the charge distribution multisite complexation model (CD-MUSIC) (Stachowicz et al., 2008; Hiemstra, 2018; Stolze et al., 2019). One of the most used techniques to relate the models with empirical observations is the ATR-FTIR (Attenuated total reflectance/Fourier transform infrared spectroscopy), since it provides information about the chemical bonds involved in the ion adsorption process (Peak et al., 1999; Arai and Sparks, 2001; Yan and Jing, 2018; Xu et al., 2019).

We sought to evaluate the intensities of inner sphere adsorption of  $\text{PO}_4$  and  $\text{SO}_4$  onto synthetic goethite samples under different experimental conditions (pH, goethite purity, and contact times) and to establish the mechanisms and models involved in those bonds. The interaction of two pH values and two oxyanions allowed the combined discussion of the effect of pH on the degree of protonation of ferrol groups and the activation energy of oxyanion to break the Fe-OH bond on the surface of the goethite.

Both chemical and physical analysis supported this study: chemical - adsorbed by inner sphere with lower energy (extraction with  $\text{HNO}_3$   $1 \text{ mol L}^{-1}$ ) and, extraction of total oxyanion adsorbed by inner sphere by EPA3051A; physical - vibrational spectroscopy (ATR-FTIR). Goethite was chosen as the adsorbent because it is the most abundant Fe oxide in soils; phosphate and sulfate were chosen to study due to the greater environmental and agronomic importance of inner-sphere complexation of those oxyanions. The hypothesis of the present study was that the mechanisms of inner-sphere complexation of  $\text{PO}_4$  and  $\text{SO}_4$  occur as a function of the protonation intensities of the surface ferrol groups (varying with pH:  $-\text{FeOH}_2^{+0.5}$ ,  $-\text{Fe-OH}^{0.5}$ , or  $-\text{FeO}^{-1.5}$ ), which define Fe-O bond strength, the contact time of the oxyanion with the hydroxylated surface, and the ligand exchangeability of the oxyanion.

## MATERIALS AND METHODS

### Goethite synthesis

Goethite was synthesized following Schwertmann and Cornell (1991), with modifications: 180 mL of  $\text{KOH}$   $3.5 \text{ mol L}^{-1}$  was added to 100 mL of  $\text{FeCl}_3 \cdot 6\text{H}_2\text{O}$   $1.0 \text{ mol L}^{-1}$ , under constant stirring; the volume of the mixture was completed to 2 L with ultrapure water ( $18.2 \text{ M}\Omega \cdot \text{cm}$  at  $25 \text{ }^\circ\text{C}$  - Millipore Direct-Q System) while maintaining agitation. The final mixture was held in an oven at  $70 \text{ }^\circ\text{C}$  for 72 h, the residue was then washed five times with 200 mL of ultrapure water, dried at  $40 \text{ }^\circ\text{C}$  for 72 h, macerated, and sieved through 0.02 mm mesh.

### Purification of synthetic goethite

Part of the synthetic goethite was purified using ammonium oxalate (AO) solution (1:25)  $0.2 \text{ mol L}^{-1}$  at pH 3 in the absence of light, stirring for 2 h (McKeague and Day, 1966), resulting in two synthetic goethite samples: i) Gt - without purification with AO; and ii) GtAO - which was AO purified.

### Saturation of Gt and GtAO with P and S

Approximately 5.00 g of Gt and GtAO (both in triplicate) were separately mixed (non-competitive saturation) with 150 mL of a  $20.000 \text{ mg P or S L}^{-1}$  solution, prepared with  $\text{KH}_2\text{PO}_4$  or  $\text{K}_2\text{SO}_4$ . Those procedures resulted in samples highly saturated with P and S ( $600 \text{ g of P or S kg}^{-1}$  of goethite). This excess of P or S guaranteed the saturation of all the outer and inner-sphere goethite adsorption sites.

This saturation procedure with P or S was repeated under the following conditions: two pH values (5.0 or 9.0), two stirring times at pH 5.0 [a 24 h short cycle (sc), or a 240 h long cycle (lc)], and only one stirring time at pH 9.0 (240 h - lc). The short cycle suspensions were stirred at 100 rpm for 24 h. For the saturation of the suspensions in the long cycle, the samples were stirred at 100 rpm for 240 h, adopting periodic cycles of 20 h of agitation followed by 4 h rest periods. The pH adjustments were made using appropriate volumes of  $\text{HNO}_3$   $0.5 \text{ mol L}^{-1}$  or  $\text{NaOH}$  solutions, checked and corrected at the end of each stirring time cycle if necessary. Saturations were carried out in the complete absence of light to avoid the influence of microbes.

At pH 5.0, approximately 100 % of the P and S are in their  $\text{H}_2\text{PO}_4^-$  ( $\text{PO}_4$ ) and  $\text{SO}_4^{2-}$  ( $\text{SO}_4$ ) forms, respectively (Lindsay, 1979). At pH 9.0, all of the S is in the  $\text{SO}_4^{2-}$  ( $\text{SO}_4$ ) form and about 98 % of the P is in the  $\text{HPO}_4^{2-}$  ( $\text{PO}_4$ ) form, with 2 % as  $\text{H}_2\text{PO}_4^-$  ( $\text{PO}_4$ ) (Lindsay, 1979). The pH values of 5.0 and 9.0 were chosen as the pH of the zero-point charges of Fe oxides ( $\text{pH}_{\text{zpc}}$ ) is near 8.5 (Costa and Bigham, 2009; Kosmulski, 2018): at pH 5.0 there is predominance of  $-\text{FeOH}_2^{+0.5}$  and at pH 9.0 there is a higher occurrence of  $-\text{FeO}^{-1.5}$  on the goethite surface, which allowed us to verify the effects of the protonation intensity of the ferrol group on Fe-O binding strength.

After the saturation steps with  $\text{PO}_4$  and  $\text{SO}_4$ , the samples were transferred to cellulose dialysis membranes (Sigma-Aldrich, reference number D9527) and immersed in ultrapure water for 21 days, with a daily renewal of the water – a procedure designed to remove excess  $\text{PO}_4$  and  $\text{SO}_4$  in solution. The samples were subsequently dried at 40 °C and sieved through 0.2 mm mesh.

### **Extraction of $\text{PO}_4$ and $\text{SO}_4$ adsorbed by outer-sphere**

To remove outer-sphere adsorbed  $\text{PO}_4$  or  $\text{SO}_4$ , the samples were subjected to the following sequential extractions: 1) approximately 4.00 g of samples saturated with  $\text{PO}_4$  or  $\text{SO}_4$  were stirred for 1 h at 100 rpm with 80 mL of  $\text{Ca}(\text{NO}_3)_2 \cdot 4\text{H}_2\text{O}$  0.5 mol L<sup>-1</sup> (Andrade et al., 2009); the suspensions were then centrifuged at 3000 rpm for 10 min and the supernatant discarded; this extraction procedure was repeated a second time; 2) the residue was subsequently submitted to double anion exchange resin extraction (Mckean and Warren, 1996; Rheinheimer et al., 2000, with adaptations) involving the goethite samples being stirred with 160 mL of ultrapure water and resin plates (AR103 QDP 434 IONICS INC. - 8.5 × 5 cm, 42.5 cm<sup>2</sup>) that have been functionalized with 160 mL  $\text{NaHCO}_3$  of 0.5 mol L<sup>-1</sup>; the resin plates were then recovered, and the goethite suspensions centrifuged at 3000 rpm for 10 min; the residues were subsequently dried at 40 °C, ground, and sieved through 0.2 mm mesh. With the extraction of exchangeable forms (outer sphere) by sequential extractions with  $\text{Ca}(\text{NO}_3)_2$  and anion exchange resin extraction, the quantities of  $\text{PO}_4$  or  $\text{SO}_4$  adsorbed on the inner-sphere goethite could then be determined.

### **Extraction of $\text{PO}_4$ and $\text{SO}_4$ adsorbed on the inner-sphere goethite**

#### ***Removal using $\text{HNO}_3$ 1 mol L<sup>-1</sup> in a closed system***

This procedure was performed according to the methodology proposed by Melo et al. (2016). Approximately 0.2500 g of each goethite sample was placed in a teflon tube (in triplicate) together with 9 mL of  $\text{HNO}_3$  1 mol L<sup>-1</sup>. The tubes were hermetically sealed and held in a microwave oven (Mars Xpress 6, CEM) for 5 min and 30 s, until the temperature reached 100 °C; that temperature was maintained for an additional period of 4 min and 30 s at 800 psi of pressure. The extracts were then filtered through slow filter paper (Macherey Nagel®), and the P and S contents were determined using inductively coupled plasma-optical emission spectroscopy (ICP-OES). The operational conditions of the ICP-OES with an axial configuration were: radiofrequency power – 1200 W; replicates – 3; plasma gas flow rate – 15 L min<sup>-1</sup>; auxiliary gas flow rate – 1.5 L min<sup>-1</sup>; sample uptake rate – 1.0 mL min<sup>-1</sup>; nebulizer gas flow rate – 0.5 L min<sup>-1</sup>; nebulizer pressure – 200 kPa; nebulizer type – seaspray; torch type – quartz; spray chamber – cyclonic; injector tube diameter – 1.2 mm; signal integration time – 15 s; analytical lines – P = 213.618 nm and S = 181.972 nm. The solid residues were recovered from the filter paper using water jets and dried at 40 °C (Melo et al., 2016).

#### ***Removal using EPA 3051A ( $\text{HNO}_3/\text{HCl}$ - 3:1)***

This procedure was performed according to the methodology proposed by Usepa (1998). Approximately 0.4000 g of each sample (in triplicate) were transferred to a teflon tube with 9.0 mL of concentrated  $\text{HNO}_3$  and 3.0 mL of concentrated  $\text{HCl}$ . The tubes were sealed and kept in a microwave oven (Mars Xpress 6, CEM) for 8 min and 40 s to raise their temperature to 175 °C; that temperature was maintained for an additional period of 4 min and 30 s. The extracts were then filtered through slow filter paper (Macherey Nagel®) and the levels of P and S were subsequently determined by inductively coupled plasma-optical emission spectroscopy (ICP-OES) as described above.

### **X-ray diffractometry (XRD) (powder samples)**

The following samples were characterized by XRD: Gt, GtAO, samples saturated with P or S, and the residues of extractions with  $\text{HNO}_3$  1.0 mol L<sup>-1</sup>, to verify the purity of the goethite

in the saturated samples. The analyses were performed in a Panalytical X'Pert<sup>3</sup> powder X-ray diffractometer (vertical goniometer), with a scan speed of  $0.4\text{ }^{\circ}2\theta\text{ s}^{-1}$  and a scanning range of  $10\text{ to }60\text{ }^{\circ}2\theta$ . The diffractometer, equipped with a graphite monochromator, CuK $\alpha$  radiation and Ni filter, was generated at 40 kV and 40 mA. A Spinner sampler was used and XRD Data Collection Software and High Score Plus (PAN Analytical) was employed for reading and processing the data.

### Specific Surface Area (SSA)

The SSA of Gt and GtAO saturated with P and S, for characterization and comparison with the non-saturated goethites, were determined by the BET method (Brunauer-Emmett-Teller) using N<sub>2</sub> adsorption, Quantachrome™ Nova Stacion C 4000e Surface Area and Pore Analyzer equipment and the Nova Win software. Approximately 0.1000 g of each sample were weighed and transferred to tubes and taken to the stations to be degassed for 8 h at 60 °C.

### Attenuated total reflectance/Fourier transform infrared spectroscopy (ATR - FTIR)

The following samples were selected to characterize the types of inner-sphere bonds (monodentate or bidentate) formed by the saturation of goethite with PO<sub>4</sub> or SO<sub>4</sub>: 1) GtAO pH 5, saturated with PO<sub>4</sub> or SO<sub>4</sub> by long cycle mixing; and 2) GtAO pH 9 saturated with PO<sub>4</sub> or SO<sub>4</sub> by long cycle mixing. Sample sets 1) and 2) were also analyzed after extracting inner-sphere adsorbed PO<sub>4</sub> or SO<sub>4</sub> with HNO<sub>3</sub> 1.0 mol L<sup>-1</sup>.

The ATR-FTIR spectra were collected between 4000 and 400 cm<sup>-1</sup> using the ATR accessory in a Bruker Invenio® R spectrometer at a resolution of 2 cm<sup>-1</sup>. All spectra were collected and processed for absorbance using Opus 8.1 software; the spectrum range of interest was selected manually using Origin® 8.5 software in the region between 1200 to 950 cm<sup>-1</sup> and between 1300 to 950 cm<sup>-1</sup>, where bands associated with the various characteristic vibrations of phosphate and sulfate occur respectively (Wijnja and Schulthess, 2000; Lefèvre, 2004).

### Scanning electron microscopy (SEM)

The raw samples of synthetic goethite were photographed in a scanning electron microscope (SEM) model Tescan Vega 3, operated at 15 kV.

## RESULTS

### Goethite sample characterizations

The same XRD patterns can be seen with Gt, GtAO, and samples saturated with P and S (Figure 1). Goethite can be classified as crystalline orthorhombic (JCPDS 29-0713) with cell parameters a, b, and c equal to 0.4608, 0.9956, and 0.302 nm, respectively (Jaiswal et al., 2013; Mohamed et al., 2017). A peak observed only in the Gt sample at  $28.4\text{ and }40.6\text{ }^{\circ}2\theta$  (CuK $\alpha$  radiation) can be attributed to sylvite (Sv - KCl), a mineral formed during goethite synthesis. In the other treatments, extraction with AO and saturation with P or S solubilized the sylvite and purified the Gt samples.

The specific surface areas (SSA) of Gt and GtAO were  $32.9\text{ and }32.6\text{ m}^2\text{ g}^{-1}$ , respectively. On average, the SSA of the samples saturated with PO<sub>4</sub> (pH 5 and 9) was  $41.6\text{ m}^2\text{ g}^{-1}$ , while the SSA of samples saturated with SO<sub>4</sub> was  $37.4\text{ m}^2\text{ g}^{-1}$ . The inner-sphere complexation of PO<sub>4</sub> or SO<sub>4</sub> made the surface relief of the goethite more irregular, increasing its SSA.

Scanning electron micrographs show the crystals with acicular morphology (greater growth towards the c axis) (Figure 2). Tests performed by Cornell and Schwertmann (2003), under the same conditions as the present study, also formed acicular crystals.

### Inner-sphere complexation of $\text{H}_2\text{PO}_4^-/\text{HPO}_4^{2-}$ and $\text{SO}_4^{2-}$ (generically treated as $\text{PO}_4$ and $\text{SO}_4$ )

The highest P content extracted with the  $\text{HNO}_3$   $1 \text{ mol L}^{-1}$  solution (P- $\text{HNO}_3$ ) was in the GtAO pH 5 lc treatment (mean of  $830.7 \text{ mg kg}^{-1}$ ) (Figure 3a). That content was almost six times higher than the same treatment at pH 9.0 (Gt pH 9 lc) ( $143.0 \text{ mg kg}^{-1}$ ). The longer contact time of the goethite samples with the concentrated  $\text{PO}_4$  solution (long cycle treatments - lc) favored the inner-sphere complexation process. The GtAO pH 5 lc adsorbed almost twice as much  $\text{PO}_4$  as GtAO pH 5 sc (Figure 3a). The inner-sphere complexation of  $\text{PO}_4$

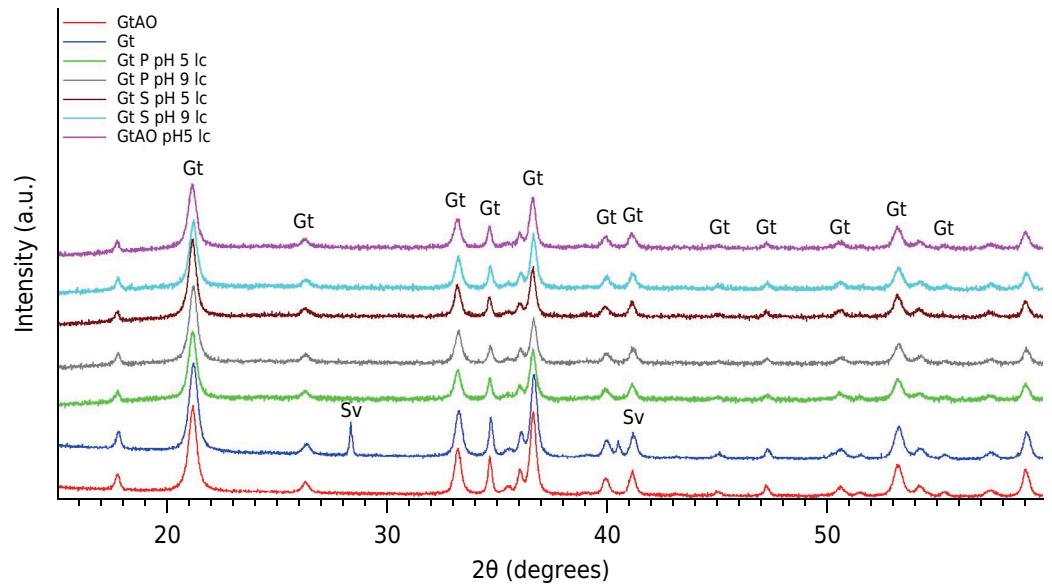


**Figure 1.** X-ray diffraction patterns (powder method and Cuka radiation) of representative samples of goethite and goethite saturated with P or S at different pHs. LEGEND: GtAO: goethite treated with ammonium oxalate (AO); Gt: goethite without AO treatment; Gt P pH 5 lc: goethite without AO treatment, saturated with P, pH adjusted to 5.0, and with a long saturation cycle (240 h); S: goethite saturated with S; pH 9: pH adjusted to 9.0; Sv: sylvite.

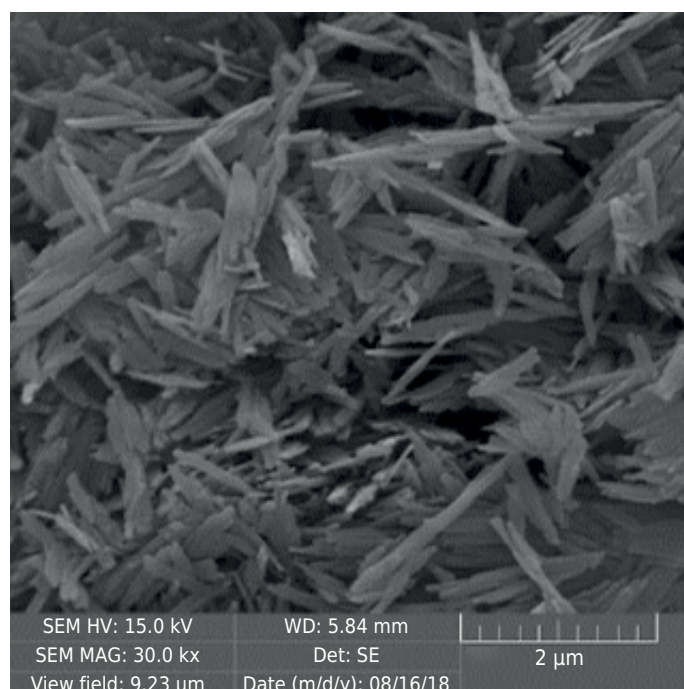
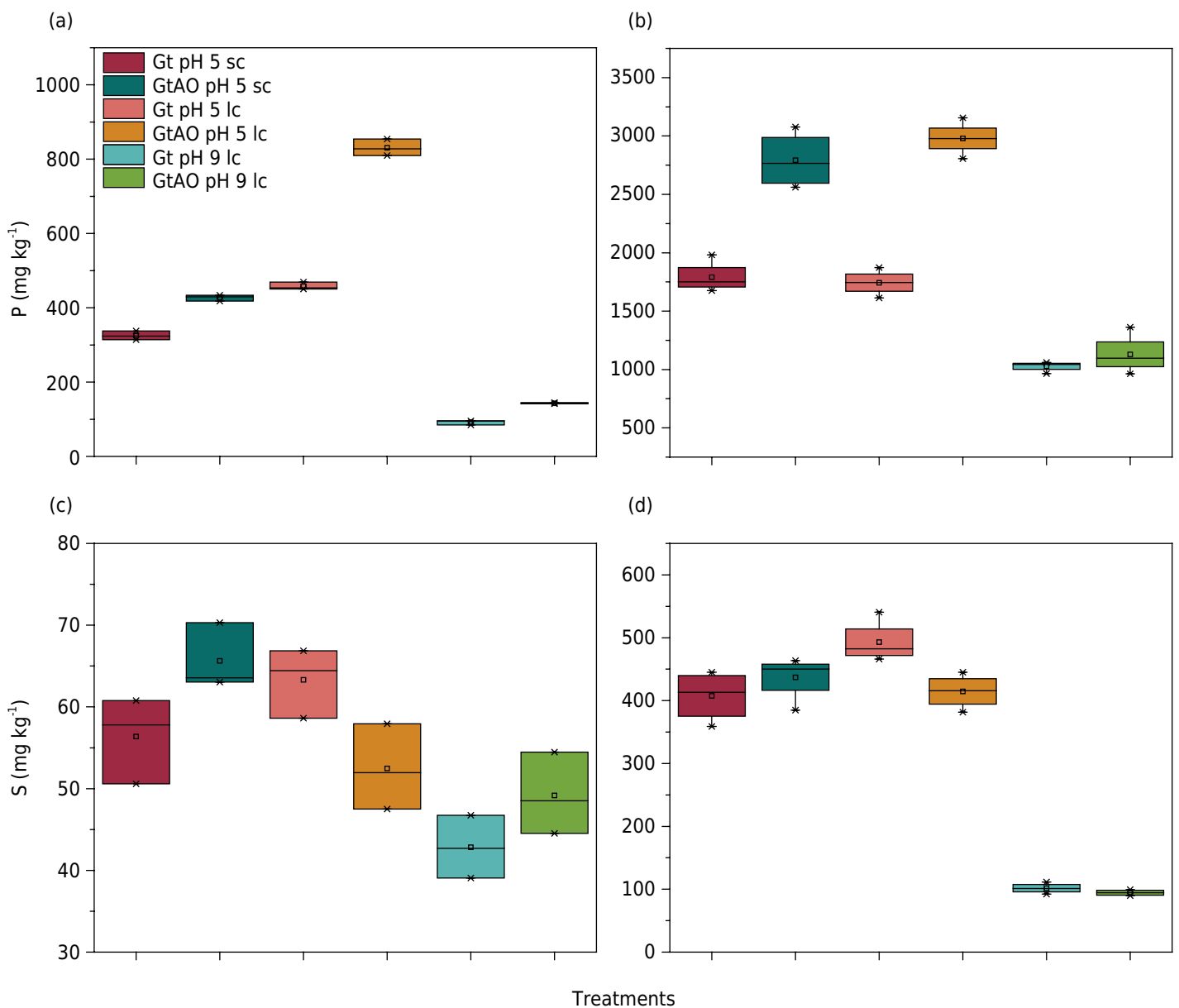


**Figure 2.** Micrography (SEM) of raw synthetic goethite.

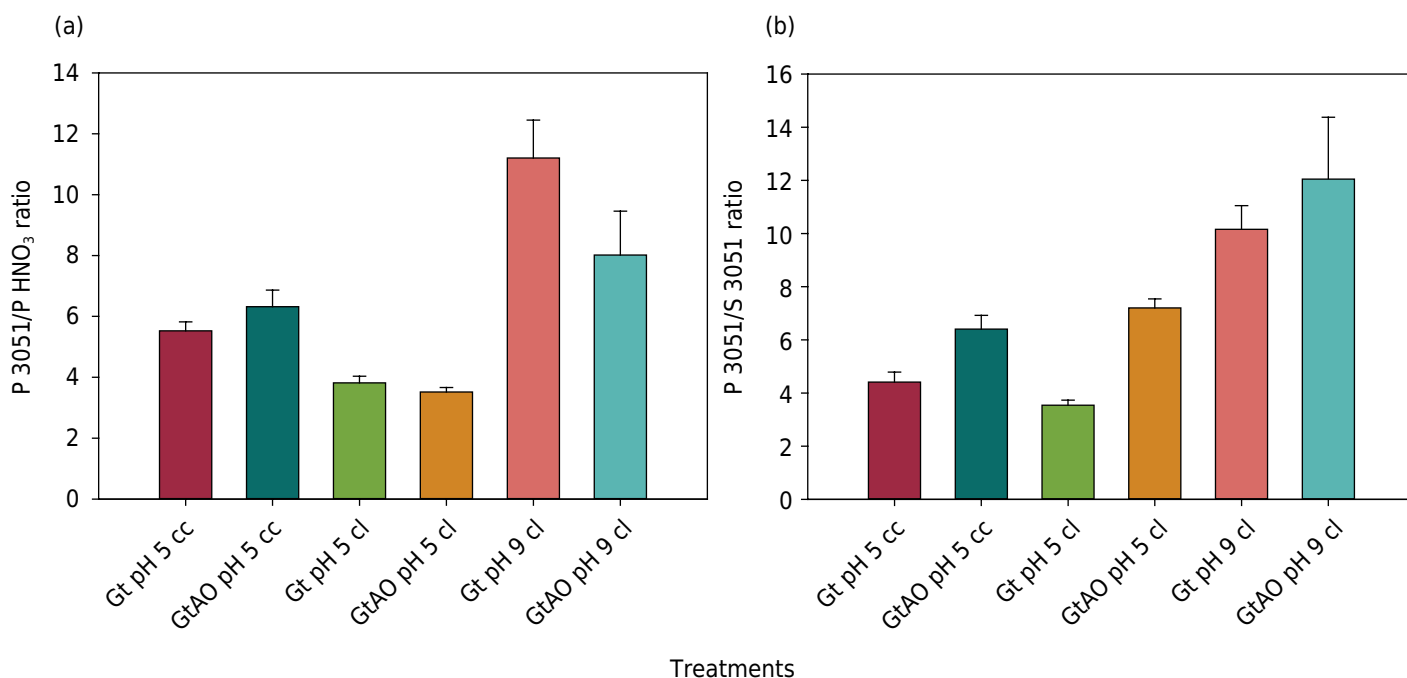
in GtAO (purified sample) was considerably higher than in Gt, principally in the long saturation cycle (Figure 3a).

The P contents adsorbed on the inner sphere extracted by 3051A (Figure 3b) were higher than the contents extracted by  $\text{HNO}_3$  (Figure 3a). Overall, the Box Plot scatters of the 3051A and  $\text{HNO}_3$  extract treatments were very similar. The most significant difference using 3051A was the proximity of short and long cycle saturations treatments for both Gt and GtAO samples.

The ratios of P-3051A (higher energy)/P- $\text{HNO}_3$  (lower energy) were calculated to evaluate the intensity of the Fe-O-P bond (strength of the inner-sphere complexation) (Figure 4a). The ratios for all treatments were greater than 1. Comparisons of the two sets of experiments, in which the only variable was pH (GtAO pH 5 lc and Gt pH 5 lc versus GtAO pH 9 lc and Gt pH 9 lc), showed the P-3051A/P- $\text{HNO}_3$  ratios to be expressively higher at pH 9.



**Figure 3.** Box-plots of the inner-sphere adsorbed P (a, b) and S (c,d) contents obtained by extraction using  $\text{HNO}_3$  1 mol L<sup>-1</sup> (a, c), and EPA 3051A (b, d) methods in samples of the different treatments. The small square inside the box plots represents the average of the triplicates of the  $\text{HNO}_3$  1 mol L<sup>-1</sup> method and quadruplicates of the EPA 3051A method, while the line indicates the median. Gt pH 5 sc: goethite without AO treatment, pH adjusted to 5.0 and short cycle saturation (24 h); GtAO: AO treated goethite, pH adjusted to 9.0; lc: long cycle saturation (240 h).



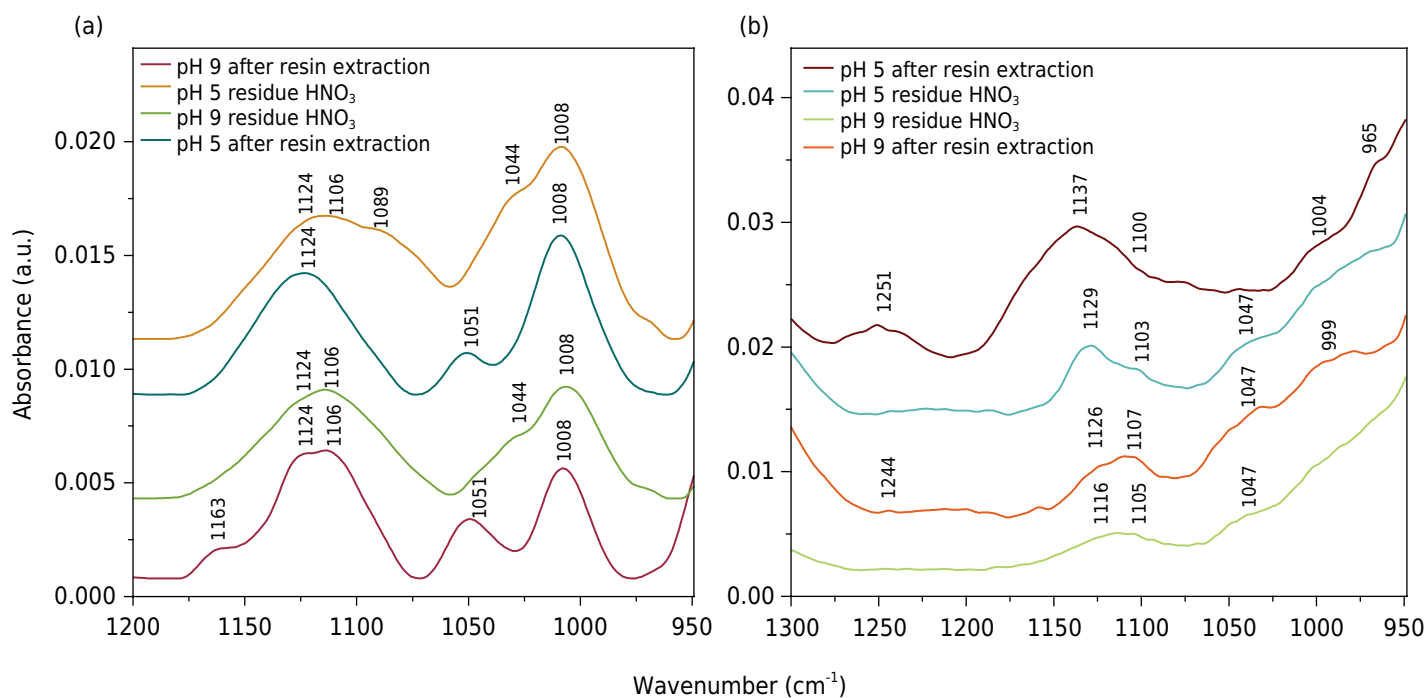
**Figure 4.** (a) Ratios of P inner sphere adsorbed contents obtained by extractions using EPA 3051A and HNO<sub>3</sub> 1.0 mol L<sup>-1</sup>. Gt pH 5 cc: goethite without AO treatment, pH adjusted to 5.0 and short cycle saturation (24 h); GtAO: Goethite treated with AO, pH adjusted to 9.0, and lc: long cycle saturation (240 h); (b) Ratios of P and S inner-sphere adsorbed contents obtained by the EPA 3051A extraction method. Gt pH 5 sc: goethite without AO treatment, pH adjusted to 5.0, and short cycle saturation (24 h); GtAO: Goethite treated with AO; lc: long cycle saturation (240 h), and pH adjusted to 9.0

Figure 5a shows the spectra obtained by attenuated total reflectance infrared spectroscopy (ATR-FTIR) analysis of the goethite samples saturated with PO<sub>4</sub> (pH 5 and pH 9) after each extraction: Ca(NO<sub>3</sub>)<sub>2</sub> + anion exchange resin (pH 5 and 9), followed by HNO<sub>3</sub> 1.0 mol L<sup>-1</sup> extraction (pH 5 and 9).

The spectral profiles of the samples extracted with HNO<sub>3</sub> are very similar and differ from the profiles of samples extracted with Ca(NO<sub>3</sub>)<sub>2</sub> + ion exchange resin (which are also similar to each other). All the spectra had in common intense bands at 1008 and 1124 cm<sup>-1</sup>. Both bands are attributed to protonated bidentate bonds (strong inner sphere adsorption) between PO<sub>4</sub> (pH 5 and 9) in goethite: the most intense band at 1008 cm<sup>-1</sup> is attributed to asymmetric (P-OFe) type stretching, and the band at 1124 cm<sup>-1</sup> to (P=O) type stretching (Tejedor-Tejedor and Anderson, 1990; Luengo et al., 2006; Rahnemaie et al., 2007). In addition to those two bands, the spectra of the HNO<sub>3</sub>-treated samples showed bands at 1106, 1089 and 1044 cm<sup>-1</sup> that can be assigned to P-O type stretching in non-protonated bidentate type bonds (Luengo et al., 2006; Rahnemaie et al., 2007).

The highest average S content extracted by HNO<sub>3</sub> was in the GtAO pH 5 sc treatment (65.6 mg kg<sup>-1</sup>), while the lowest average content was obtained in the Gt pH 9 lc treatment (42.8 mg kg<sup>-1</sup>) (Figure 3c). The GtAO adsorbed more SO<sub>4</sub> than Gt only at pH 5 in the short cycle saturation (Gt pH 5 sc versus GtAO pH 5 sc, and Gt pH 9 lc versus GtAO pH 9 lc). When comparing the two adsorption cycles at pH 5, however, Gt in the long cycle demonstrated better adsorption conditions (Gt pH 5 lc).

The Gt pH 5 lc and GtAO pH 9 lc treatments had the maximum (492.9 mg kg<sup>-1</sup>) and the minimum average S contents by 3051A extraction (94.4 mg kg<sup>-1</sup>) respectively (Figure 3d). As in the P saturation experiments, the pH of the medium was the main variable influencing the inner-sphere complexation reactions of SO<sub>4</sub>. At the pH 5, the influence of the two saturation cycle durations (sc or lc), as well as goethite type (Gt or GtAO) with 3051A extraction (Figure 3d) were similar to those observed for S extraction with HNO<sub>3</sub> (Figure 3c). At pH 9, the Gt treatment resulted in the highest adsorption of SO<sub>4</sub>.



**Figure 5.** Spectra of the attenuated total reflectance infrared spectroscopy (ATR-FTIR) analyses of the solids corresponding to P (a) and S (b) -saturated goethite after extractions with: anion exchange resin - pH 5 after resin extraction (pH adjusted to 5.0 at saturation) and pH 9 after resin extraction (pH adjusted to 9.0 at saturation) and  $\text{HNO}_3$  1.0 mol  $\text{L}^{-1}$  (pH 5 residue  $\text{HNO}_3$  and pH 9 residue  $\text{HNO}_3$ ).

The ratios of the average P contents and average S contents adsorbed on the inner-sphere and extracted by 3051A were calculated (Figure 4b). Those P/S ratios were greater than 1 under all of the different experimental conditions. In the long cycle, the total inner-sphere complexation (P/S ratio) at pH 5 was approximately four times higher in Gt and approximately seven times higher in GtAO. At pH 9 those ratios rise to 10 and 12, respectively.

Figure 5b shows the spectra obtained from the attenuated total reflectance infrared spectroscopy (ATR-FTIR) analysis of goethite samples saturated with  $\text{SO}_4$  (pH 5 and pH 9) after each extraction:  $\text{Ca}(\text{NO}_3)_2$  + anion exchange resin (pH 5 and 9) and after extraction with  $\text{HNO}_3$  1.0 mol  $\text{L}^{-1}$  (pH 5 and 9). The 1047 and 1251  $\text{cm}^{-1}$  bands are assigned to the asymmetric stretching modes of the  $\text{n}_3(\text{S}-\text{O})$  type of binuclear bidentate inner-sphere complexes (Wijnja and Schulthess, 2000). The band at 1251  $\text{cm}^{-1}$  observed in the solid at pH 5 after resin treatment disappears when the solid is treated with  $\text{HNO}_3$ . The 1137 and 1129  $\text{cm}^{-1}$  bands are attributed to monodentate inner-sphere bonds between sulfate and goethite (Peak et al., 1999; Wijnja and Schulthess, 2000).

## DISCUSSION

### General discussion

The saturation of goethite with 600 g  $\text{kg}^{-1}$  of P and S, after dialysis pretreatments, resulted in the maximum contents of the forms adsorbed by outer sphere (sum of the two extractions with  $\text{Ca}(\text{NO}_3)_2$  and two extractions with anion exchange resin) of 107 and 1050 mg  $\text{kg}^{-1}$  of P and S, respectively. After all these pretreatments, the maximum contents adsorbed by inner sphere were only 3000 and 500 mg  $\text{kg}^{-1}$  of P and S, respectively (Figures 3b and 3d). These data show that the idealization of the adsorption test with high doses of P and S to guarantee the complete saturation of the adsorption sites by inner sphere and the washing of these oxyanions with dialysis for three weeks and the sequential extractions with  $\text{Ca}(\text{NO}_3)_2$  and anion resin were adequate.

Inner-sphere P adsorption was higher in treatments at pH 5 than in pH 9 (Figures 3a and 3b) due to relative increases in less-reactive negatively charged functional groups ( $\text{Fe-OH}^{-0.5}$  and  $\text{Fe-O}^{-1.5}$ ) at the higher pH. The inner-sphere complexation process can be explained by the concept of ligand exchange, when a hydroxyl group is exchanged for an oxyanion (Acelas et al., 2013). Three types of functional groups can be found on the goethite surface:  $\text{Fe-OH}_2^{+0.5}$ ,  $\text{Fe-OH}^{-0.5}$ , and  $\text{Fe-O}^{-1.5}$ . The monoprotonated group ( $\text{Fe-OH}^{-0.5}$ ) prevails in both pH 5 and 9 (Boily et al., 2001), but there is a relative increase in the form  $\text{Fe-O}^{-1.5}$  at pH 9. Biprotonated  $\text{Fe-OH}_2^{+0.5}$  and  $\text{Fe}_3\text{OH}^{+0.5}$  groups are more significant at acidic pH (Antelo et al., 2005). Phosphate is adsorbed in the Stern layer by electrostatic interactions when the pH is acidic, due to anion exchange capacities (AEC) on the Gt surface (outer-sphere complexation). In the next step,  $\text{PO}_4$  loses its hydration water and moves from the Stern layer to an intramicellar position, forming covalent Fe-O-P bonds (inner-sphere complexation). The  $-\text{OH}_2$  ligand bound to iron (III) in  $\text{Fe-OH}_2^{+0.5}$  is unstable and easily exchangeable by  $\text{PO}_4$  (Acelas et al., 2013). An inner-sphere complex is formed by monodentate or bidentate bonds. At low pH, bidentate bonding is more likely to occur with  $\text{PO}_4$ , as there is a higher probability of displacement of two  $-\text{OH}_2^{+0.5}$  ligands (Acelas et al., 2013). Thus, ligand exchange is attributed only to the  $\text{Fe-OH}^{-0.5}$  and  $\text{Fe-OH}_2^{+0.5}$  groups.

The longer contact time ( $t_c$ ) of goethite samples with the concentrated  $\text{PO}_4$  solution favored the inner-sphere complexation process (Figures 3a and 3b), with the  $\text{PO}_4$  ions distributed in the Diffuse Layer and Stern Layer (outer-sphere complexation) (Rahnemaie et al., 2006). The volumes of the ions are considered in this theory, and therefore only a small number of ions  $\text{PO}_4$  can be accommodated in the Stern layer due to its finite thickness ( $d_{\text{stern}}$ ) (Brown et al., 2016). Only this  $\text{PO}_4$  from the Stern Layer in contact with the goethite surface can lose hydration water, promote ligand exchange, and establish inner-sphere complexation with Fe. Another  $\text{PO}_4$  can then enter the Stern Layer and follow the same inner-sphere complexation procedure. Therefore, the access of  $\text{PO}_4$  ions to the particle surface (the passage from the diffuse to the Stern layer) requires time (Strauss et al., 1997).

The inner-sphere complexation of  $\text{PO}_4$  onto GtAO was higher than onto Gt, especially in the long saturation cycle (Figures 3a and 3b). Treatment with ammonium oxalate (AO) favored goethite purification by, for example, removing the sylvite formed during its synthesis (Figure 1). The P contents absorbed on the inner-sphere and extracted by 3051A were higher than those extracted by  $\text{HNO}_3$  1 mol  $\text{L}^{-1}$  (Figure 3b). The 3051A method (higher energy) extracted the inner-sphere adsorbed P having higher binding energy in a thermodynamically more stable, bidentate-like form (Acelas et al., 2013). The release of P or S by  $\text{HNO}_3$  1.0 mol  $\text{L}^{-1}$  acid in a closed system involves hydrolysis reactions that attack the external layers of those soil minerals, while the 3051A method promotes total goethite solubilization (Guedes et al., 2020; Melo et al., 2016).

The P-3051A and P- $\text{HNO}_3$  ratios (Figure 4a) were greater than 1 in all treatments - showing that a more aggressive extraction method is required to remove all of the P adsorbed on the inner-sphere of the goethite. Comparing the two sets of experiments, where pH was the only variable (GtAO pH 5  $t_c$  and Gt pH 5  $t_c$  versus GtAO pH 9  $t_c$  and Gt pH 9  $t_c$ ), the P-3051A/P- $\text{HNO}_3$  ratios were expressively higher in the pH 9 treatments, suggesting that inner-sphere complexations are weaker or more easily disrupted when P is in the  $\text{H}_2\text{PO}_4^-$  form predominant between pH 2.1 and 7.2 (Lindsay, 1979). At pH 5, due to higher  $\text{H}^+$  activity, protonation of the oxygen of the Fe-O-P bond occurs, which changes the excess charge of this oxygen from -0.5 to +0.5 (Figures 6a and b). In that configuration, the excess positive charge and the proton shifts the electronic density of the Fe-O bond toward the oxygen (Figure 6b) - a shift that weakens the Fe-O bond and favors the hydrolysis promoted by the  $\text{HNO}_3$  1.0 mol  $\text{L}^{-1}$  solution (a lower P-3051A/P- $\text{HNO}_3$  ratio at pH 5 - Figure 4a). On the other hand, protonation is not favored at pH 9, and the electronic density is shifted more to the central position of the bond - which strengthens

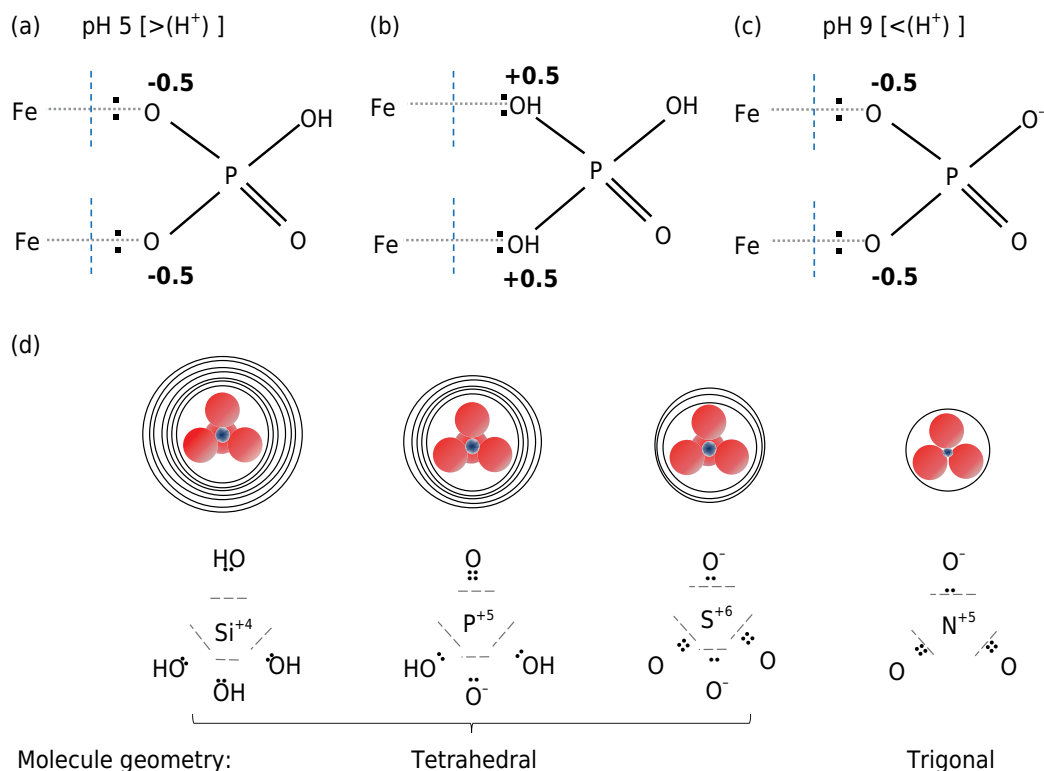


**Figure 6.** (a, b and c) Models of the bidentate bond structures from the saturation experiments of Gt pH 5 - goethite (no OA treatment) and GtAO - goethite (OA-treated sample) with pH set to 5.0 (a) and (b) and pH set to 9.0 (c). Gray dotted lines represent the chemical bonds between Fe and O; dashed blue lines represent the middle of the bond between Fe and O; two vertical dots represent the pair of electrons shared between the Fe and O of the ferrol groups; (d) Schematic spatial representation of  $H_4SiO_4$ ,  $H_2PO_4^-$ ,  $SO_4^{2-}$  and  $NO_3^-$ . Rings around the species represent the surface negative charge density of each geometry and its ability to exchange ligands upon inner-sphere complexation. The closer the electron pair is to the surface of the geometry, the higher the electron density near the OH or O. The dashed gray lines represent half of the distance of the chemical bond between the cation and the oxygen.

the Fe-O bond (Figure 6c). Inner-sphere complexation is lower at pH 9, but its bond is stronger than pH 5.

These structural models agree with the bands observed in the ATR-FTIR spectra (Figure 5a). In general, the spectra of all samples (after resin extraction and in the  $HNO_3$  residue, at both pH values) indicate the formation of both inner and outer-sphere complexes with the ligand in its protonated and unprotonated bidentate form.

The  $Fe-OH_2^{+0.5}$  group also favored ligand exchange with  $SO_4$  (greater inner-sphere complexation at pH 5) (Figures 3c and 3d). The ATR-FTIR spectra (Figure 5b) at pH 5, after the two extractions (by resin and by  $HNO_3$  1 mol  $L^{-1}$ ) indicate that monodentate and bidentate inner-sphere type bonds remained. Only the bidentate inner-sphere bonds remained after extractions at pH 9. The P/S ratios (Figure 4b) were greater than 1 in all the different experiments, showing the higher adsorption capacity of  $PO_4$  as compared to  $SO_4$  - thus demonstrating the lower ligand exchange strength of  $SO_4$  relative to  $PO_4$ , mainly above neutral pH.

For the discussion of ATR-FTIR spectra, it is interesting to use the approach of comparison between the vibrational modes of free ligand anions in the face of post-coordination modes for selenate and sulfate (Wijnja and Schulthess, 2000). In addition to the simple association with vibrational modes, it is also possible to relate the bands with the symmetry of the anions. Both free phosphate and sulfate present symmetry  $T_d$ . When coordinated in the monodentate form, there is a reduction for  $C_{3v}$  symmetry, splitting the  $\nu_3$  mode in two bands. When coordinated in bidentate form, symmetry is reduced to  $C_{2v}$ ,

with  $\nu_3$  mode being split into three new bands (Nakamoto, 1997; Wijnja and Schulthess, 2000). For uncoordinated sulfate, a band at  $1100\text{ cm}^{-1}$  corresponding to asymmetric stretching mode of the  $\nu_3(\text{S-O})$  is observed, which splits in the bands shown in  $1040$ ,  $1150$  and  $1250\text{ cm}^{-1}$  for a coordination of the bidentate type and  $1070$  and  $1130\text{ cm}^{-1}$  for monodentate coordination (Hug, 1997). Several of such bands are evidenced in the spectra of figure 5b, which illustrate the presence of both the coordination of the bidentate and monodentate inner sphere, and also by the outer sphere.

There is also a difference related to  $\text{PO}_4$ , in which the outer-sphere complexation bands are not observable after the extraction procedures, being predominantly retained by inner-sphere complexation. Besides that, it is interesting to note that a mixture of outer and inner-sphere complexes also occurs with ferrihydrite, but at  $\text{pH} < 7$  (also below the point of zero charge) instead  $\text{pH} 5$ , indicating the different behavior of those two iron oxyhydroxides towards sulfate (Liu et al., 2018).

## Models and Mechanisms of inner-sphere complexation

### Related to goethite surfaces

It is possible to predict the displacement of the electron pair in a bond based on electronegativity. The electron pair in Fe-O is positioned closer to the oxygen due to its higher electronegativity ( $\chi = 3.4$ ) as compared to Fe ( $\chi = 1.8$ ), although the two protons in the  $\text{Fe-OH}_2^{+0.5}$  group attract the electron pair even more toward the oxygen (Figure 7a). Additionally, the two protons generate an excess positive charge (+0.5), which also plays a role in attracting the electron pair toward the oxygen. In the non-protonated ferrol group ( $\text{Fe-O}^{-1.5}$ ), the H is absent, and the electron pair moves closer to the center of the bond (Figure 7c) - a configuration that increases the covalent character of the bond and makes it more difficult to break. The  $\text{Fe-OH}^{-0.5}$  group represents an intermediate situation (Figure 7b). Therefore, the electronegativity data of the three types of ferrol groups allows us to establish the following sequence of ease of formation of inner-sphere complexation with oxyanions by ligand exchange:  $\text{Fe-OH}_2^{+0.5} \gg \text{Fe-OH}^{-0.5} \gg \text{Fe-O}^{-1.5}$ .

### Related to the ligand exchange capacity of the oxyanion

The inner-sphere complexation between a metal oxide and an oxyanion can be classified as an acid-base reaction. The central atom of the Fe oxide in that reaction behaves as a Lewis acid (an electron pair receptor) while the oxygens of the oxyanion behave as electron-pair donors (Lewis bases) (Acelas et al., 2013). Because of the instability of the  $-\text{OH}_2^{+0.5}$  ligand, its exchange by another Lewis base (ligand) is facilitated (Sparks, 2003). The principle of inner-sphere complexation is that the oxyanion ( $\text{PO}_4$  and  $\text{SO}_4$  in the present study) has sufficient basicity, based on its negative charge density, to break the metal-oxygen bond and form a surface complex and release water (Kubicki et al., 2007). After breaking this bond, the oxyanion binds directly to Fe through electron pair sharing with the oxygen of the oxyanion (inner-sphere complexation).

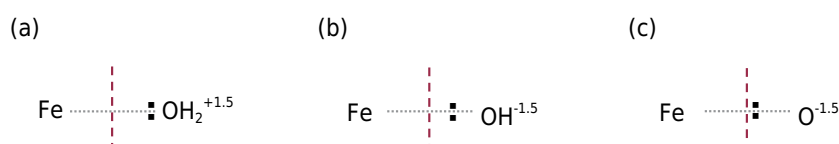


**Figure 7.** Schematic representation of the different protonations of the ferrol group based on the displacement of the electron pairs of the Fe-O bonds. (a) diprotonated ferrol group; (b) protonated ferrol group; (c) deprotonated ferrol group. Dotted gray lines represent the chemical bond between Fe and O; dashed blue lines represent the middle of the bond between Fe and O; two vertical dots represent the electron pairs shared between Fe and the ferrol groups.

The inclusion of  $\text{SiO}_4$  in the oxyanion inner-sphere complexation model (Figure 6d) is due to previous research that demonstrated that its inner-sphere complexation intensity is equal or slightly higher than that of  $\text{PO}_4$  (Hiemstra, 2018; Hilbrandt et al., 2019). At the other extreme,  $\text{NO}_3^-$  is quantitatively the principle anionic soil nutrient, and its inner-sphere complexation capacity on soil colloids is unfavorable compared to other oxyanions (Acelas et al., 2017).

In addition to those structures, the difference in electronegativity ( $\Delta\chi$ ) between the central cation and the oxygen of the oxyanions also defines the different intensities of inner-sphere oxyanion adsorption, as they determine the strength of the Lewis base or ligand. Covalent bonds have unequal sharing of electron pairs between the atoms, so that one of them develops a positive partial charge ( $\delta^+$ ) while the other becomes more electronegative and will more strongly attract the electron pair to itself and acquire a partial negative charge ( $\delta^-$ ) that creates an inductive effect in the molecule (Macedo and Haiduke, 2020).

The electronegativity difference of P-O in  $\text{PO}_4$  is 1.2 ( $\chi_{\text{O}} - \chi_{\text{P}} = 3.4 - 2.2 = 1.2$ ), while the S-O in sulfate has  $\Delta\chi = 0.8$  ( $\chi_{\text{O}} (3.4) - \chi_{\text{S}} (2.6)$ ) (Huheey et al., 1979), which means that the inductive effect caused by oxygen in P-O is more intense than in S-O (greater displacement of the electronic pair of the P-O bond toward the O of the tetrahedron surface). The density of negative charges toward the oxygen, in addition to facilitating electron pair donation to Fe (monodentate bond formation), confers a greater covalent character to the adjacent P-OH bond (Macedo and Haiduke, 2020). This higher negative charge density on the surface of the P tetrahedral, relative to the S tetrahedral, allows the former oxyanion to promote ligand exchange with  $-\text{OH}_2^{+0.5}$  and  $-\text{OH}^{-0.5}$  from the goethite surface. Sulfate, on the other hand, would have energy sufficient only to exchange the  $-\text{OH}_2^{+0.5}$  group. Thus,  $\text{PO}_4$  are stronger Lewis bases than  $\text{SO}_4$  and will form bonds with greater covalent characters with Lewis acids (such as the Fe in goethite). Following this same reasoning, the electronic pairs of the Si tetrahedra ( $\text{Si} = 1.9$ ) are even more displaced toward the oxygen ( $\delta^-$ ) and  $\text{H}_4\text{SiO}_4$  has its greatest distribution of electrons at the edge of the tetrahedral - which gives it greater negative surface charge density ( $\delta^-$ ) and a greater capacity for electron sharing (strong Lewis base) - and therefore a greater capacity for exchanging ferrol groups (Figure 6d). This does not occur with  $\text{NO}_3^-$  because  $\Delta\chi$  is small in N-O (Huheey et al., 1979).

Another important characteristic is the positive charge density of the  $\text{Si}^{4+}$  core, which is better protected by the four oxygens of the tetrahedral than the higher charge of the  $\text{S}^{6+}$ . The  $\text{S}^{6+}$  tetrahedral has the lowest surface negative charge density and the least strength to promote breakage of the Fe-OH bond of goethite at both ends of the tetrahedral geometry. In addition to the more unfavorable positioning of its electronic pairs (farther from the surface of the oxyanion - Figure 6d),  $\text{N}^{5+}$  is stabilized in a trigonal planar geometry. As that geometry is only two-dimensional, the charge of the  $\text{N}^{5+}$  core has no protection and is projected outward, further reducing the negative charge density of this oxyanion. The order of inner-sphere complexation reactivity of the oxyanions reported in this model follows the sequence (from most reactive to least reactive):  $\text{SiO}_4 > \text{PO}_4 \gg \text{SO}_4 \gg \text{NO}_3$ .

### Related to pH 5 and 9

The most favorable configuration for inner-sphere complexation will be at pH 5 for  $\text{PO}_4$  in the  $-\text{Fe}-\text{OH}_2^{+0.5}$  group of goethite, while the most unfavorable situation will be at pH 9 for  $\text{SO}_4$  in the  $-\text{Fe}-\text{O}^{-1.5}$  group. As a model of the inner-sphere complexation for these two oxyanions we therefore have: i)  $\text{PO}_4$  inner-sphere complexation occurs at low (5.0) and basic pH values (9.0) with  $-\text{FeOH}_2^{+0.5}$  and  $-\text{FeOH}^{-0.5}$ ; ii)  $\text{SO}_4$  inner-sphere complexation occurs both at low (5.0) and basic (9.0) pH values only with the  $-\text{FeOH}_2^{+0.5}$  group. The surface charge densities of both oxyanions are insufficient to break the bonds of the fully deprotonated ferrol groups ( $-\text{FeO}^{-1.5}$ ). Examples of the inner-sphere complexation of  $\text{PO}_4$  at pH 9 on the  $-\text{FeOH}_2^{+0.5}$  and  $-\text{FeOH}^{-0.5}$  groups for binuclear bidentate bond formation are

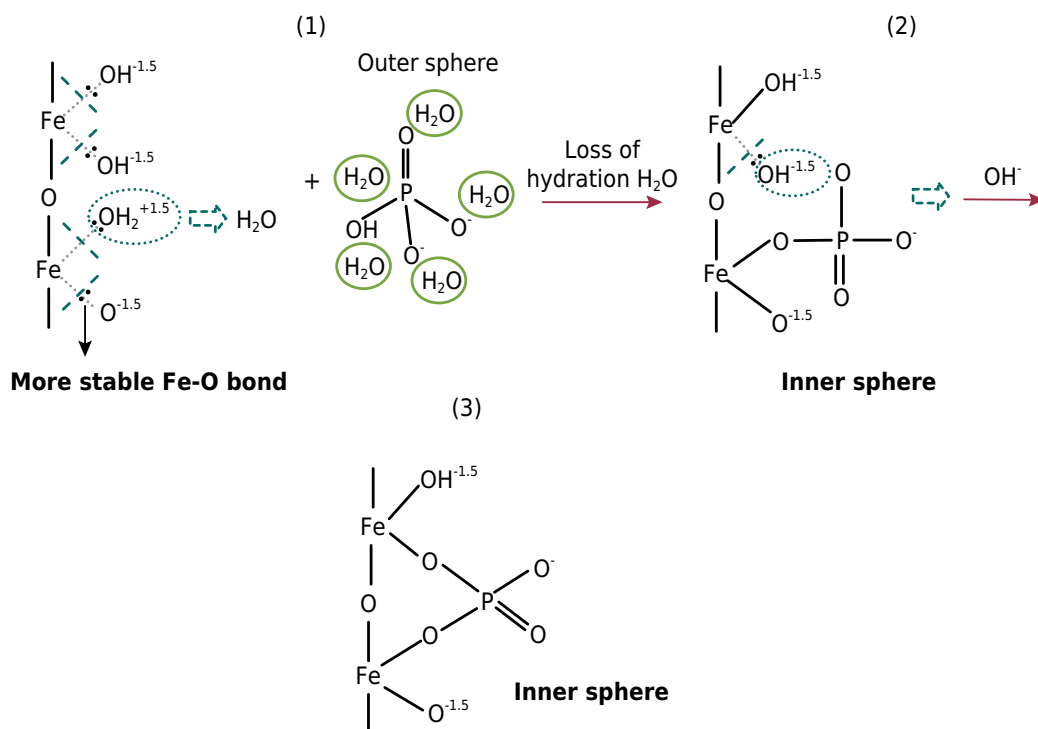


**Figure 8.** Example of inner-sphere complexation of  $\text{PO}_4$  at pH 9 on the goethite surface (binuclear bidentate bond formation).

shown in figure 8. As the density of sulfate reactive functional groups ( $-\text{OH}_2^{+0.5}$ ) becomes reduced at pH 9 (lower probability of occurrence of two such adjacent groups), only monodentate bonding on the goethite surface is expected for  $\text{SO}_4$ .

## CONCLUSION

Purification of goethite with ammonium oxalate increased inner-sphere adsorption of  $\text{H}_2\text{PO}_4^-/\text{HPO}_4^{2-}$  and  $\text{SO}_4^{2-}$  (generically treated as  $\text{PO}_4$  and  $\text{SO}_4$ ). A longer contact time favored the passage of oxyanions from the Stern layer to the intramacellar portion (outer sphere to inner sphere adsorption). Oxyanion inner-sphere complexation at pH 5 is much more expressive than at pH 9. Inner-sphere complexation of  $\text{PO}_4$  at pH 5 and 9 on goethite occur with bidentate binuclear protonated and bidentate binuclear deprotonated forms respectively. The deprotonated form at pH 9 increases the strength and the stability of Fe-O-P binding.

Inner-sphere complexation of  $\text{PO}_4$  was much more expressive compared to  $\text{SO}_4$ . Phosphorus and S oxyanions displace the deprotonated ferrol ligand ( $-\text{OH}_2^{+0.5}$  in  $-\text{FeOH}_2^{+0.5}$ ), while the  $-\text{OH}^{-0.5}$  in the  $-\text{Fe-OH}^{-0.5}$  group is displaced only by  $\text{PO}_4$ . The  $-\text{O}^{-1.5}$  ligand in  $\text{Fe-O}^{-1.5}$  group is not displaced by  $\text{PO}_4$  or  $\text{SO}_4$  on goethite. The high negative surface charge density of  $\text{PO}_4$  defined its greater activation energy to exchange the  $-\text{OH}_2^{+0.5}$  and  $-\text{OH}^{-0.5}$  in the goethite surface in relation to  $\text{SO}_4$ . Overall, inner sphere oxyanion adsorption on goethite depends on the level of ferrol protonation (variable as function of pH) and the activation energy of the oxyanion. As a practical result to increase the P fertilization efficiency, we recommend applying phosphate only after correcting soil acidity with limestone, which will increase the relative density of iron groups without protonation ( $\text{Fe-O}^{-1.5}$ ).

## AUTHOR CONTRIBUTIONS

**Conceptualization:** Antônio Carlos Vargas Motta (equal), Carla Gomes de Albuquerque (equal), Fabiana Gavelaki (equal) and Vander de Freitas Melo (equal).

**Data curation:**  Carla Gomes de Albuquerque (equal) and  Fabiana Gavelaki (equal).

**Formal analysis:**  Aldo José Gorgatti Zarbin (equal),  Carla Gomes de Albuquerque (equal),  Caroline Mariano Ferreira (equal) and  Fabiana Gavelaki (equal).

**Funding acquisition:**  Antônio Carlos Vargas Motta (equal) and  Vander de Freitas Melo (equal).

**Investigation:**  Carla Gomes de Albuquerque (equal),  Fabiana Gavelaki (equal) and  Vander de Freitas Melo (equal).

**Methodology:**  Carla Gomes de Albuquerque (equal),  Fabiana Gavelaki (equal) and  Vander de Freitas Melo (equal).

**Project administration:**  Vander de Freitas Melo (lead).

**Resources:**  Antônio Carlos Vargas Motta (equal) and  Vander de Freitas Melo (equal).

**Supervision:**  Antônio Carlos Vargas Motta (equal) and  Vander de Freitas Melo (equal).

**Visualization:**  Carla Gomes de Albuquerque (lead).

**Writing - original draft:**  Carla Gomes de Albuquerque (equal) and  Fabiana Gavelaki (equal).

**Writing - review & editing:**  Aldo José Gorgatti Zarbin (equal),  Antônio Carlos Vargas Motta (equal),  Caroline Mariano Ferreira (equal) and  Vander de Freitas Melo (equal).

## REFERENCES

- Abdala DB, Northrup PA, Arai Y, Sparks DL. Surface loading effects on orthophosphate surface complexation at the goethite/water interface as examined by extended X-ray Absorption Fine Structure (EXAFS) spectroscopy. *J Colloid Interf Sci.* 2015;437:297-303. <https://doi.org/10.1016/j.jcis.2014.09.057>
- Acelas NY, Hadad C, Restrepo A, Ibarguen C, Flórez E. Adsorption of nitrate and bicarbonate on Fe-(Hydr)oxide. *Inorg Chem.* 2017;56:5455-64. <https://doi.org/10.1021/acs.inorgchem.7b00513>
- Acelas NY, Mejia SM, Mondragón F, Flórez E. Density functional theory characterization of phosphate and sulfate adsorption on Fe-(hydr)oxide: Reactivity, pH effect, estimation of Gibbs free energies, and topological analysis of hydrogen bonds. *Comput Theor Chem.* 2013;1005:16-24. <https://doi.org/10.1016/j.comptc.2012.11.002>
- Alleoni LRF, Melo VF, Rocha WSD. Eletroquímica, adsorção e troca iônica no solo. In: Melo VF, Alleoni LRF, editors. *Química e mineralogia do solo: Aplicações.* Viçosa, MG: Sociedade Brasileira de Ciência do Solo; 2009. v. 2. p. 70-120.
- Anderson SJ, Sposito G. Cesium-adsorption method for measuring accessible structural surface charge. *Soil Sci Soc Am J.* 1991;55:1569-76. <https://doi.org/10.2136/sssaj1991.03615995005500060011x>
- Andrade MG, Melo VF, Souza LCP, Gabardo J, Reissmann CB. Metais pesados em solos de área de mineração e metalurgia de chumbo. II - Formas e disponibilidade para plantas. *Rev Bras Cienc Solo.* 2009;33:1889-97. <https://doi.org/10.1590/S0100-06832009000600038>
- Antelo J, Avena M, Fiol S, López R, Arce F. Effects of pH and ionic strength on the adsorption of phosphate and arsenate at the goethite-water interface. *J Colloid Interf Sci.* 2005;285:476-86. <https://doi.org/10.1016/j.jcis.2004.12.032>
- Arai Y, Sparks DL. ATR-FTIR spectroscopic investigation on phosphate adsorption mechanisms at the ferrihydrite-water interface. *J Colloid Interf Sci.* 2001;241:317-26. <https://doi.org/10.1006/jcis.2001.7773>

- Boily J-F, Lützenkirchen J, Balmès O, Beattie J, Sjöberg S. Modeling proton binding at the goethite ( $\alpha$ -FeOOH)-water interface. *Colloid Surface A*. 2001;179:11-27. [https://doi.org/10.1016/S0927-7757\(00\)00712-3](https://doi.org/10.1016/S0927-7757(00)00712-3)
- Brown MA, Goel A, Abbas Z. Effect of electrolyte concentration on the stern layer thickness at a charged interface. *Angew Chem*. 2016;55:3790-4. <https://doi.org/10.1002/anie.201512025>
- Cornell RM, Schwertmann U. The iron oxides: Structure, properties, reactions, occurrences and uses. 2nd ed. Weinheim: Wiley-VCH; 2003. <https://doi.org/10.1002/3527602097>
- Costa ACS, Bigham JM. Óxidos de ferro. In: Melo VF, Alleoni LRF, editors. Química e mineralogia do solo: Conceitos básicos. Viçosa, MG: Sociedade Brasileira de Ciência do Solo; 2009. v. 1. p. 506-20.
- Essington ME, Stewart MA. Adsorption of antimonate, sulfate, and phosphate by goethite: Reversibility and competitive effects. *Soil Sci Soc Am J*. 2018;82:803-14. <https://doi.org/10.2136/sssaj2018.01.0003>
- Fang D, Zhao Z, Chang E, Xu R, Hong Z, Zhou L, Jiang J. Paddy cultivation significantly alters phosphorus sorption characteristics and loss risk in a calcareous paddy soil chronosequence. *Soil Sci Soc Am J*. 2019;83:575-83. <https://doi.org/10.2136/sssaj2018.09.0320>
- Gérard F. Clay minerals, iron/aluminum oxides, and their contribution to phosphate sorption in soils - A myth revisited. *Geoderma*. 2016;262:213-26. <https://doi.org/10.1016/j.geoderma.2015.08.036>
- Gu C, Wang Z, Kubicki JD, Wang X, Zhu M. X-ray absorption spectroscopic quantification and speciation modeling of sulfate adsorption on ferrihydrite surfaces. *Environ Sci Technol*. 2016;50:8067-76. <https://doi.org/10.1021/acs.est.6b00753>
- Guedes LG, Melo VF, Batista AH. The classic aqua regia and EPA 3051A methods can mislead environmental assessments and certifications: Potentially harmful elements desorption in short-range order materials. *Chemosphere*. 2020;251:126356. <https://doi.org/10.1016/j.chemosphere.2020.126356>
- Hiemstra T. Ferrihydrite interaction with silicate and competing oxyanions: Geometry and Hydrogen bonding of surface species. *Geochim Cosmochim Ac*. 2018;238:453-76. <https://doi.org/10.1016/j.gca.2018.07.017>
- Hilbrandt I, Lehmann V, Zietzschmann F, Ruhl AS, Jekel M. Quantification and isotherm modelling of competitive phosphate and silicate adsorption onto micro-sized granular ferric hydroxide. *RSC Adv*. 2019;9:23642-51. <https://doi.org/10.1039/c9ra04865k>
- Hinkle MAG, Wang Z, Giammar DE, Catalano JG. Interaction of Fe(II) with phosphate and sulfate on iron oxide surfaces. *Geochim Cosmochim Ac*. 2015;158:130-46. <https://doi.org/10.1016/j.gca.2015.02.030>
- Hug S. *In situ* fourier transform infrared measurements of sulfate adsorption on hematite in aqueous solutions. *J Colloid Interf Sci*. 1997;188:415-22. <https://doi.org/10.1006/jcis.1996.4755>
- Huheey JA, Keiter EA, Keiter RL. Bonding models in inorganic chemistry: 2. The covalent bond. In: Huheey JE, Keiter EA, Keiter RL, editors. *Inorganic chemistry: Principles of structure and reactivity*. 4th ed. New York: Harper Collins; 1979. p. 182.
- Jaiswal A, Banerjee S, Mani R, Chattopadhyaya MC. Synthesis, characterization and application of goethite mineral as an adsorbent. *J Environ Chem Eng*. 2013;1:281-9. <https://doi.org/10.1016/j.jece.2013.05.007>
- Kim J, Li W, Philips BL, Grey CP. Phosphate adsorption on the iron oxyhydroxides goethite ( $\alpha$ -FeOOH), akaganeite ( $\beta$ -FeOOH), and lepidocrocite ( $\gamma$ -FeOOH): A  $^{31}\text{P}$  NMR Study. *Energy Environ Sci*. 2011;4:4298-305. <https://doi.org/10.1039/c1ee02093e>
- Kosmulski M. The pH dependent surface charging and points of zero charge. VII. Update. *Adv J Colloid Interf Sci*. 2018;251:115-38. <https://doi.org/10.1016/j.cis.2017.10.005>
- Kubicki JD, Kwon KD, Paul KW, Sparks DL. Surface complex structures modelled with quantum chemical calculations: Carbonate, phosphate, sulphate, arsenate and arsenite. *Eur J Soil Sci*. 2007;58:932-44. <https://doi.org/10.1111/j.1365-2389.2007.00931.x>
- Kubicki JD, Paul KW, Kabalan L, Zhu Q, Mroziak MK, Aryanpour M, Strongin DR. ATR-FTIR and density functional theory study of the structures, energetics, and vibrational spectra of phosphate adsorbed onto goethite. *Langmuir*. 2012;28:14573-87. <https://doi.org/10.1021/la303111a>

- Lefèvre G. In situ Fourier-transform infrared spectroscopy studies of inorganic ions adsorption on metal oxides and hydroxides. *Adv Colloid Interfac.* 2004;107:109-23. <https://doi.org/10.1016/j.cis.2003.11.002>
- Li Z, Arai Y. Comprehensive evaluation of mineral adsorbents for phosphate removal in agricultural water. *Adv Agron.* 2020;164:93-159. <https://doi.org/10.1016/bs.agron.2020.06.003>
- Lindsay WL. Phosphates and sulfur. In: Lindsay WL. *Chemical equilibria in soils.* New York, John Wiley; 1979. p. 168-281.
- Liu J, Zhu R, Liang X, Ma L, Lin X, Zhu J, He H, Parker SC, Molinari M. Synergistic adsorption of Cd(II) with sulfate/phosphate on ferrihydrite: An in situ ATR-FTIR/2D-COS study. *Chem Geol.* 2018;477:12-21. <https://doi.org/10.1016/j.chemgeo.2017.12.004>
- Luengo C, Brigante M, Antelo J, Avena M. Kinetics of phosphate adsorption on goethite: Comparing batch adsorption and ATR-IR measurements. *J Colloid Interf Sci.* 2006;300:511-8. <https://doi.org/10.1016/j.jcis.2006.04.015>
- Macedo GK, Haiduke RLA. A quantum theory atoms in molecules study about the inductive effect of substituents in methane derivatives. *ACS Omega.* 2020;15:9041-5. <https://doi.org/10.1021/acsomega.0c01081>
- McKeague JA, Day JH. Dithionite- and oxalate-extractable Fe and Al as aids in differentiating various classes of soils. *Can J Soil Sci.* 1966;46:13-22. <https://doi.org/10.4141/cjss66-003>
- McKean SJ, Warren GP. Determination of phosphate desorption characteristics in soils using successive resin extractions. *Commun Soil Sci Plan.* 1996;27:2397-417. <https://doi.org/10.1080/00103629609369711>
- Melo VF, Batista AH, Gilkes RJ, Rate AW. Relationship between heavy metals and minerals extracted from soil clay by standard and novel acid extraction procedures. *Environ Monit Assess.* 2016;188:668. <https://doi.org/10.1007/s10661-016-5690-8>
- Mohamed R, El-Maghrabi HH, Riad M, Mikhail S. Environmental friendly FeOOH adsorbent materials preparation, characterization and mathematical kinetics adsorption data. *J Water Process Eng.* 2017;6:212-22. <https://doi.org/10.1016/j.jwpe.2017.01.005>
- Nakamoto K. *Infrared and raman spectra of inorganic and coordination compounds. Part B: Applications in coordination, organometallic, and bioinorganic chemistry.* 5th ed. New York: Wiley-Interscience; 1997.
- Peak D, Ford RG, Sparks DL. An in-situ ATR-FTIR investigation of sulfate bonding mechanisms on goethite. *J Colloid Interf Sci.* 1999;218:289-99. <https://doi.org/10.1006/jcis.1999.6405>
- Persson P, Nilsson N, Sjöberg S. Structure and bonding of orthophosphate ions at the iron oxide-aqueous interface. *J Colloid Interf Sci.* 1996;177:263-75. <https://doi.org/10.1006/jcis.1996.0030>
- Rahnemaie R, Hiemstra T, Van Riemsdijk WH. Geometry, charge distribution, and surface speciation of phosphate on goethite. *Langmuir.* 2007;23:3680-9. <https://doi.org/10.1021/la062965n>
- Rahnemaie R, Hiemstra T, Van Riemsdijk WH. Inner- and outer-sphere complexation of ions at the goethite-solution interface. *J Colloid Interf Sci.* 2006;297:379-88. <https://doi.org/10.1016/j.jcis.2005.11.003>
- Rheinheimer DS, Anghinoni I, Kaminski J. Depleção do fósforo inorgânico de diferentes frações provocada pela extração sucessiva com resina em diferentes solos e manejos. *Rev Bras Cienc Solo.* 2000;24:345-54. <https://doi.org/10.1590/S0100-06832000000200012>
- Roberts TL, Johnston AE. Phosphorus use efficiency and management in agriculture. *Resour Conserv Recy.* 2015;105:275-81. <https://doi.org/10.1016/j.resconrec.2015.09.013>
- Scherer HW. Sulfur in soils. *J Plant Nutr Soil Sc.* 2009;172:326-35. <https://doi.org/10.1002/jpln.200900037>
- Schwertmann U, Cornell RM. *Iron oxides in the laboratory: Preparation and characterization.* Weinheim: Wiley-VCH; 1991.
- Schwertmann U, Taylor RM. Iron oxides. In: Dixon JB, Weed SB, editors. *Minerals in soil environments.* Madison: Soil Science Society of America; 1989. p. 379-438.

- Sparks DL. Sorption phenomena on soils. In: Sparks DL, editor. Environmental soil chemistry. 2nd ed. Amsterdam: Academic Press; 2003. p. 132-86. <https://doi.org/10.1016/B978-012656446-4/50005-0>
- Stachowicz M, Hiemstra T, Riemsdijk WH. Multi-competitive interaction of As(III) and As(V) oxyanions with  $\text{Ca}^{2+}$ ,  $\text{Mg}^{2+}$ ,  $\text{PO}_4^{3-}$ , and  $\text{CO}_3^{2-}$  ions on goethite. *J Colloid Interf Sci*. 2008;320:400-14. <https://doi.org/10.1016/j.jcis.2008.01.007>
- Stolze L, Zhang D, Guo H, Rolle M. Surface complexation modeling of arsenic mobilization from goethite: Interpretation of an in-situ experiment. *Geochim Cosmochim Acta*. 2019;248:274-88. <https://doi.org/10.1016/j.gca.2019.01.008>
- Strauss R, Brümmer GW, Barrow NJ. Effects of crystallinity of goethite: II. Rates of sorption and desorption of phosphate. *Eur J Soil Sci*. 1997;48:101-14. <https://doi.org/10.1111/j.1365-2389.1997.tb00189.x>
- Tejedor-Tejedor MI, Anderson MA. Protonation of phosphate on the surface of goethite studied by CIR-FTIR and electrophoretic mobility. *Langmuir*. 1990;6:602-11. <https://doi.org/10.1021/la00093a015>
- United States Environmental Protection Agency - Usepa. SW-846 EPA method 3051A: Microwave assisted acid digestion of sediments, sludges, soils and oils. Washington, DC: US Environmental Protection Agency; 1998. Available from: <https://www.epa.gov/sites/default/files/2015-12/documents/3051a.pdf>
- Waiman CV, Avena MJ, Regazzoni AE, Zanini GP. A real time in situ ATR-FTIR spectroscopic study of glyphosate desorption from goethite as induced by phosphate adsorption: Effect of surface coverage. *J Colloid Interf Sci*. 2013;394:485-9. <https://doi.org/10.1016/j.jcis.2012.12.063>
- Wijnja H, Schulthess CP. Vibrational spectroscopy study of selenate and sulfate adsorption mechanisms on Fe and Al (hydr)oxide surfaces. *J Colloid Interf Sci*. 2000;229:286-97. <https://doi.org/10.1006/jcis.2000.6960>
- Xu J, Koopal LK, Wang M, Xiong J, Hou YL, Tan W. Phosphate speciation on Al-substituted goethite: ATR-FTIR/2D-COS and CD-MUSIC modeling. *Environmental Science Nano*. 2019;6:3625-37. <https://doi.org/10.1039/c9en00539k>
- Yan W, Jing C. Molecular insights into glyphosate adsorption to goethite gained from ATR-FTIR, two-dimensional correlation spectroscopy, and DFT study. *Environ Sci Technol*. 2018;52:1946-53. <https://doi.org/10.1021/acs.est.7b05643>
- Zhao Y, Liu F, Qin X. Adsorption of diclofenac onto goethite: Adsorption kinetics and effects of pH. *Chemosphere*. 2017;180:373-8. <https://doi.org/10.1016/j.chemosphere.2017.04.007>
- Zhao Z, Chang E, Lai P, Dong Y, Xu R, Fang D, Jiang J. Evolution of soil surface charge in a chronosequence of paddy soil derived from Alfisol. *Soil Till Res*. 2019;192:144-50. <https://doi.org/10.1016/j.still.2019.05.011>